Available online at www.sciencedirect.com

SciVerse ScienceDirect

journal homepage: www.elsevier.com/locate/he

Steam reforming of ethanol: Effects of support and additives on Ni-based catalysts

R. Trane-Restrup [a], S. Dahl [b], A.D. Jensen [a,*]

[a] Department of Chemical and Biochemical Engineering, Technical University of Denmark, Søltofts Plads, Building 229, 2800 Kgs. Lyngby, Denmark

[b] Department of Physics, Technical University of Denmark, Building 307, 2800 Kgs. Lyngby, Denmark

ARTICLE INFO

Article history:
Received 27 April 2013
Received in revised form
20 August 2013
Accepted 6 September 2013
Available online 15 October 2013

Keywords:
Steam reforming
Ethanol
Nickel
Carbon deposition
Sulfur
Additives

ABSTRACT

Steam reforming (SR) of oxygenated species like bio-oil or ethanol can be used to produce hydrogen or synthesis gas from renewable resources. However, deactivation due to carbon deposition is a major challenge for these processes. In this study, different strategies to minimize carbon deposition on Ni-based catalysts during SR of ethanol were investigated in a flow reactor. Four different supports for Ni were tested and $Ce_{0.6}Zr_{0.4}O_2$ showed the highest activity, but also suffered from severe carbon deposition at 600 °C or below. Operation at 600 °C or above were needed for full conversion of ethanol over the most active catalysts at the applied conditions. At these temperatures the offgas composition was close to the thermodynamical equilibrium. Operation at high temperatures, 700 °C and 750 °C, gave the lowest carbon deposition corresponding to 30–60 ppm of the carbon in the feed ending as solid carbon over $Ni/MgAl_2O_4$ and $Ni/Ce_{0.6}Zr_{0.4}O_2$.

Promotion of $Ni/MgAl_2O_4$ with K, CeO_2, and ZrO_2 increased conversion, decreased carbon deposition, or both. Promoting $Ni/MgAl_2O_4$ with both K and CeO_2 showed particularly promising results with high degrees of conversion and carbon deposition of less than 400 ppm of the carbon in the feed at approx. 600 °C. The different promoters did not influence the product distribution to any significant extent.

Selective poisoning with small amounts of K_2SO_4 on $Ni–CeO_2/MgAl_2O_4$ at 600 °C decreased carbon deposition from 900 to 200 ppm of the carbon in the feed. However, the yield of H_2 decreased from 80% to 64% and the yield of hydrocarbons increased from 3.5% to 12.7% when increasing the amount of K_2SO_4 on the catalyst from 0 wt% to 0.65 wt% indicating that the catalyst activity to hydrocarbon reforming decreased.

1. Introduction

Bio-oil is produced through flash pyrolysis of second generation biomass and is an interesting energy carrier with an energy density up to ten times higher than raw biomass [1,2]. Thus, an attractive concept for biomass utilization may be to produce bio-oil at regional plants close to the biomass production site and then transport it to a central processing plant

Abbreviations: HDO, hydrodeoxygenation; SR, steam reforming; WGS, water gas shift; GHSV, gas hourly space velocity; WHSV, weight hourly space velocity.

* *Corresponding author.* Tel.: +45 4525 2841; fax: +45 4588 2258.
E-mail address: aj@kt.dtu.dk (A.D. Jensen).

0360-3199/$ – see front matter
http://dx.doi.org/10.1016/j.ijhydene.2013.09.027

for upgrading to more valuable products like crude oil or synthesis gas. This concept lowers the cost of transportation associated with using biomass, making the overall process more feasible [1].

Bio-oil is an acidic mixture of many different oxygenated species, which gives the oil a lower heating value compared with fossil based fuels as well as a low storage stability with a risk of polymerization and phase separation [3–5]. The bio-oil is not suited for direct use as a fuel in engines or boilers and needs upgrading to become a valuable product. In this context catalytic processes like hydrodeoxygenation (HDO) or steam reforming (SR) are prospective upgrading options [6,7].

Hydrodeoxygenation is a process, where the bio-oil is reacted with H_2 at elevated pressures and temperatures over suitable catalysts. Oxygen is hereby removed from the oil as water rendering a crude oil like product [7,8], which can undergo well known refinery chemistry to produce diesel, kerosene, and gasoline. The H_2 needed for hydrotreating of the bio-oil can be produced through SR of bio-oil, which would make the entire process sustainable [6,9–11]. The SR of bio-oil can also be used to produce synthesis gas for Fischer–Tropsch or methanol synthesis, to produce H_2 for hydrotreating of crude oil, or for ammonia synthesis [8].

Steam reforming of bio-oil is an endothermic process conducted at high temperatures and the offgas composition is governed by the equilibrium between reforming, reaction 1, water gas shift (WGS), reaction 2, and methanation, reaction 3:

$$C_nH_mO_p + (n-p)\ H_2O \rightleftharpoons n\ CO + (n-p+m/2)\ H_2 \quad (1)$$

$$CO + H_2O \rightleftharpoons CO_2 + H_2 \quad (2)$$

$$CO + 3H_2 \rightleftharpoons CH_4 + H_2O \quad (3)$$

High temperatures will shift the reforming (reaction 1) and methanation equilibria (reaction 3) towards CO and H_2. However, at these temperatures the WGS (reaction 2) will be shifted towards CO and H_2O giving a lower yield of H_2. Therefore the maximum in hydrogen production is between 600 °C and 800 °C. However, lowering the temperature and inserting a WGS reactor after the reforming reactor can be used to obtain the desired CO/H_2-ratio in the product gas. The CO/H_2-ratio in offgas from the reformer will depend on temperature and S/C-ratio; high temperatures will increase the CO/H_2 while increasing the S/C-ratio will lower the CO/H_2-ratio at a given temperature.

Steam reforming of bio-oil and bio-oil model compounds have been investigated over both base and noble metal catalysts, where high degrees of conversion and high yields of H_2 were achieved [9–13]. The major hurdle for this process is a short lifetime of the catalysts due to carbon deposition and the main focus is therefore to find operating conditions and catalysts capable of operating with low or no carbon deposition.

One way of lowering the carbon deposition is through pretreatment of bio-oil, where the amount of char forming compounds is reduced, which lowers the risk of clogging of pipes and carbon formation prior to and within the catalytic bed. At the moment fractionation of bio-oil by water addition is used in laboratories to separate lignin-like compounds from the bio-oil and only steam reform the aqueous fraction from the separation process [9,11,14]. Dilution with methanol is also used in laboratory scale to stabilize the bio-oil and make it easier to handle and convert [15–17]. In the first strategy, carbon and hydrogen is lost in the lignin fraction, while costly methanol is applied in the second.

To understand SR of bio-oil, model compounds, like acetic acid, ethanol, and acetone, have been investigated in some detail. In this work, SR of ethanol is investigated as a model compound of bio-oil because it has a functionality which is found in bio-oil and is prone to carbon deposition [18–22]. Furthermore SR of ethanol is interesting as it can be used to provide H_2 for fuel cells in mobile applications [21].

Several catalysts have been investigated for SR of ethanol including Ni, Cu, Co, Ir, Au, Pt, Pd, Ru, and Rh on Al_2O_3 [18,23–29]; Ni, Ag, Rh, and Ru on $MgAl_2O_4$ [19,30–32]; Pt, Rh, Co, Pt, and Ir on $Ce_x\ Zr_{1-x}\ O_2$ [33–42], and several other systems like perovskites or hydrotalcites based catalysts [43,44]. For a complete overview the reader is referred to the following reviews [21,22,45,46]. As indicated above, many metals can be used in SR but Ni is one of few active metals used in conventional SR catalysts, due to the low price and good activity of Ni compared with the more expensive noble metals [47].

Magnesium or calcium aluminates are used as supports for industrial SR catalysts and have a low number of acid sites, which reduces the risk of decomposition of the oxygenates and therefore also the risk of carbon deposition [48]. Furthermore a more stable and higher activity for $MgAl_2O_4$ compared with Al_2O_3 has been reported [11,48,49]. The increased activity has been ascribed to an increased water dissociation on the support and formation of smaller metal particles [48,49]. Furthermore steam gasification of the coke might be facilitated by spillover of O- or OH-species from the support to the metal particles [48]. CeO_2 and $Ce_x\ Zr_{1-x}\ O_2$ have been reported to facilitate water dissociation and thereby supply O for oxidation of carbon on the surface due to their redox properties [34,39,50–52].

Potassium is known from conventional SR to bind to step sites on Ni particles and hereby reduce the rate of reaction but also the risk of carbon formation as carbon islands cannot grow large enough to nucleate carbon whiskers [47,53]. Results from the SR of acetic acid over K-promoted Ni/Al_2O_3 catalysts showed reduced CH_4 formation, increased activity, and lower carbon deposition [54]. An optimal loading of K was reported to be 8 wt% [54]. Results from the SR of ethanol over Ni/$MgAl_2O_4$ showed a decreased carbon deposition by a factor of 3 when doping with 1 wt% of K [19].

There is however a lack of systematic studies of catalyst formulation on carbon formation. In this work a systematic investigation of different options for lowering the rate of carbon deposition in SR of ethanol and hereby enhancing catalyst lifetime through changes in the catalyst formulation is carried out, including changing support material, adding promoters, and doping with sulfur.

2. Experimental

2.1. Catalyst preparation

Several catalysts were prepared by incipient wetness impregnation with a $Ni(NO_3)_2$-solution on four different

carriers; CeO_2 (AMR Ltd., 141 m^2/g), $Ce_{0.6}Zr_{0.4}O_2$ (AMR Ltd., 137 m^2/g), $MgAl_2O_4$, and $CeZrO_4/MgAl_2O_4$. The two latter supports were prepared in-house according to the procedure described below. $Ni(NO_3)_2 \cdot 6\,H_2O$ (Sigma–Aldrich, > 97% pure) was dissolved in a volume of water corresponding to the pore volume of the dry carrier. The solution was mixed with the dry carrier material and stirred. The wet particles were dried at 110 °C overnight and calcined at 800 °C (heating rate 10 °C/min) for 2 h in stagnant air.

Magnesium aluminate was prepared by incipient wetness impregnation of a high surface area alumina (Puralox TH 150 from SASOL Germany, 150 m^2/g) with $Mg(NO_3)_2$ as precursor. The alumina was mixed with a solution containing stoichiometric amounts of $Mg(NO_3)_2$ (Fluka, 99% pure) followed by drying at 110 °C and calcination at 900 °C (heating rate 10 °C/min) for 8 h in stagnant air.

The synthesized $MgAl_2O_4$ was co-impregnated with Ni, K, CeO_2, ZrO_2. Maximum two species were impregnated at a time, so when naming the catalysts / denotes separate impregnation while – denotes co-impregnation. After each impregnation step the catalyst was dried and after the final impregnation it was calcined at 800 °C (heating rate 10 °C/min) for 2 h. $Ce(NO_3)_3 \cdot 6H_2O$, $ZrO(NO_3)_2 \cdot H_2O$, and KNO_3 were used as precursors for CeO_2, ZrO_2, and K, respectively. The precursors were acquired from Sigma–Aldrich Ltd. and were ≥99% pure.

Sulfur addition to the catalysts was done by impregnating the calcined catalyst with a solution of K_2SO_4 or H_2SO_4 followed by drying at 110 °C overnight. The impregnation liquids had concentrations corresponding to a nominal sulfur coverage of roughly 6, 13, and 26%, which corresponded to a sulfur content of 0.03–0.12 wt%. Sulfur coverage was calculated by assuming that all the sulfur from the liquid adsorbs on the Ni particles. The number of Ni surface sites was estimated based on the particle size determined by XRD and assuming spherical particles and a Ni-atom area of $6.2 \cdot 10^{-20}$ m^2 (calculated based on a face-centered cubic nickel atom in the (100) plane).

2.2. Experimental setup

The flowsheet for the experimental setup can be seen in Fig. S.1 in Supplementary Data. The setup consisted of a gas supply section where up to eight different gases could be connected, a liquid supply section where two bubble columns were used to supply water and ethanol. Nitrogen flows were saturated with ethanol or water at 60 °C and 79 °C, respectively, in the bubble columns and led to the reactor. The gases and liquids were mixed in lines heated to 110 °C prior to entering a quartz reactor placed in a three zone furnace. After the reactor there was a condenser operated at 6–7 °C, which collected liquid samples. After the condenser the gases passed the analysis section, which consisted of a Varian MicroGC CP-4900 and a 5-channel Rosemount NGA 2000 on-line gas analyzer. The MicroGC had two columns, a molecular sieve 5A and a PoraPlot Q, and two thermal conductivity detectors (TCD), which measured the concentrations of CO, CO_2, H_2, CH_4, C_2H_4, and C_2H_6. Samples were injected to the GC every 10 min. The on-line gas analyzer measured the CO, CO_2, and O_2 concentrations continuously and data points were collected every 30 s. Data from the GC was used to determine the product distribution and representative measurements every approx. 30 min are used to show trends and deactivation.

The catalyst was placed between two pieces of quartz wool resting on a quartz frit inside a quartz tube with an inner diameter of 17 mm placed in the furnace. The steam and ethanol was fed from the top of the reactor through an inlet tube with an outer diameter of 6 mm and perforated with 12 holes in the end to distribute the gas over catalyst bed. The outlet of the inlet/feeding tube was approx. 50 mm above the catalyst bed. The temperature was measured by a thermocouple placed in a pocket just below the quartz frit.

Analysis of the liquid from the condenser was conducted by a Shimadzu GCMS/FID-QP2010 UltraEi fitted with a Supelco Equity-5 column. Identification was made on the mass spectrometer (MS) and quantification was done on the flame ionization detector (FID).

2.2.1. Catalytic test

0.5 g of catalyst with d_p = 410–725 μm was loaded into the reactor and then heated to 600 °C in a flow of N_2. At 600 °C the flow was changed to a 50/50 flow of N_2 and H_2 of roughly 500 NmL/min for 1 h to reduce the NiO to Ni. After reduction the reactor was purged with N_2 for 10 min and then the reactants were directed to the reactor. The total feed flow rate was about 1500 NmL/min and had an approximate composition of 3.2–3.5% of ethanol, 38.6–39.2% of water (corresponding to a molar ratio of steam to carbon (S/C-ratio) of roughly 6), and N_2 as balance. The pressure was atmospheric and temperature varied between 400 and 750 °C.

The conversion and carbon deposition were quite reproducible and the standard deviation on conversion was generally ±2% while carbon deposition had a relative standard deviation of ±10%.

Estimations based on Weisz–Prater and Mears criteria showed that diffusion was not limiting for the overall reaction with the applied particle sizes and experimental conditions. Furthermore experiments with d_p = 410–725 μm and d_p = 250–410 μm showed similar results with respect to conversion and carbon deposition.

2.2.2. Determination of the amount of carbon deposited

The amount of carbon deposited during an experiment was determined by cooling the reactor to 200 °C and then heating the spent catalysts to 700 °C (10 °C/min) in a 1 NL/min flow of 2–3% O_2 in N_2. The evolution of CO and CO_2 was monitored by the on-line gas analyzer (data points every 5 s) and the amount of carbon on the catalyst was determined by integration of these signals.

2.3. Catalyst characterization

The BET surface area of all the prepared catalysts was measured by N_2 adsorption at its boiling point using multipoint BET theory with seven points in the p/p_0 = 0.05–0.3 range using a Quantachrome iQ2.

XRD-spectra were recorded for spent and fresh catalyst powders by a PANalytical X'Pert PRO Diffractometer, which had a rotating sample holder, a rotating copper anode X-ray source, nickel filter, and automatic anti-scatter and

divergence slits. The particle size of NiO was determined by the Scherrer equation, Eq. (4) [55],:

$$d_p = \frac{K \cdot \lambda}{\beta \cdot \cos(\theta)} \quad (4)$$

Where K is a shape factor set to 0.9 [55], λ is the X-ray wavelength, β is full width at half maximum corrected for the instrumental line broadening, while θ is the Bragg angle.

Temperature controlled reduction (TPR) of the catalysts were conducted in a flow of 10% H_2 in He and the temperature was raised from room temperature to 900 °C with a temperature ramp of 5 °C/min. The concentrations of H_2O, H_2, and He were followed by a mass spectrometer.

Bright field transmission electron microscopy of fresh and spent catalysts were conducted on a Tecnai T20 G2 microscope with a thermionic-lanthanum hexaboride, LaB_6, as electron source. The fresh catalysts were reduced, cooled down, and removed from the reactor and then transported to TEM investigations. The TEM samples were crushed, slurried with ethanol and deposited on a copper grid covered with a lacey carbon film.

Elemental analysis of the catalysts was conducted by dissolving the catalyst and then use inductively coupled plasma optimal emission spectroscopy (ICP-OES).

2.4. Calculations

Space velocity (W/F) is defined as mass of catalyst pr. flow of ethanol in g/h, $F_{Eth,\,m}$:

$$W/F = \frac{m_{Cat}}{F_{Eth,m}} \quad [h] \quad (5)$$

Conversion of ethanol is calculated from the formation of products on a carbon basis as:

$$X = \frac{\sum n_{C,i} \cdot n_{i,prod}}{2 \cdot n_{C_2H_6O,in}} \cdot 100\% \quad (6)$$

Where $n_{C,\,i}$ is the number of carbon atoms in component n_i and $n_{i,\,prod}$ is the number of moles of compound i produced.

The yield of products are based on the definition by Fogler [56]:

$$Y_i = \frac{n_{C,i} \cdot n_{i,prod}}{\sum n_{C,i} \cdot n_{i,prod}} \cdot 100\% \quad (7)$$

The yield of H_2 is defined as:

$$Y_{H_2} = \frac{n_{H_2}}{6 \cdot X \cdot n_{C_2H_6O,in}} \cdot 100\% \quad (8)$$

The factor of 6 is the maximum number of H_2 moles, which can be produced from 1 mol of ethanol including full shift of CO to H_2 (see reaction 2).

Carbon deposition is reported as the amount of carbon deposited pr. amount carbon in the feed, mole C/mole C_{Feed}, and as mass of carbon deposited pr. mass of catalyst and time, mg C/(g_{Cat} × h).

3. Results and discussion

3.1. Characterization of catalysts

The nickel particle size based on XRD measurements and surface area of all the tested catalysts are shown in Table 1. The surface areas and nickel particle sizes are in the same range for all the $MgAl_2O_4$ based catalyst with values of 52–69 m^2/g and 6–9 nm, respectively. Ni/CeO_2 and Ni/$Ce_{0.6}Zr_{0.4}O_2$ both have higher surface areas and larger Ni particles with values around 90–113 m^2/g and 10–20 nm, respectively. Therefore Ni seems to be better dispersed on $MgAl_2O_4$ and $CeZrO_4/MgAl_2O_4$ compared with CeO_2 and $Ce_{0.6}Zr_{0.4}O_2$.

TEM-images of reduced Ni/$MgAl_2O_4$ and Ni/$Ce_{0.6}Zr_{0.4}O_2$ as well as particle size distribution determined from TEM-images can be seen in Fig. S.2 in Supplementary Data. For Ni/$Ce_{0.6}Zr_{0.4}O_2$ (Fig. S 2a) it is difficult to distinguish between Ni and the support, but it can be seen that the particles in general had a size of 13 nm ± 3 nm, which is slightly below the results obtained with XRD. The size distribution from the TEM-images is used to calculate the mean volume diameter, which is used for comparison. XRD was conducted on unreduced samples while the TEM was conducted on reduced samples, which could explain the difference in particle size. For Ni/$MgAl_2O_4$ (Fig. S.2c) Ni and the support can be

Table 1 – Characterization results of the fresh catalysts (Ni as NiO) prepared by calcination in stagnant air at 800 °C.

Catalyst	Promoter	Metal loading [wt%]	BET surface area [m^2/g]	$d_{p,\,Ni}$[nm]
Ni/$Ce_{0.6}Zr_{0.4}O_2$	–	8.2	90	15–20
Ni/CeO_2	–	8.2	113	10
Ni/$MgAl_2O_4$	–	8.1	69	7
Ni/$CeZrO_4$/$MgAl_2O_4$	10 wt% CeO_2 10 wt% ZrO_2	8.0	63	6
Ni–K/$CeZrO_4$/$MgAl_2O_4$	9 wt% CeO_2 9 wt% ZrO_2, 5 wt% K	8.2	47	8
Ni–K/$MgAl_2O_4$	5 wt% K	8.2	55	7
Ni–CeO_2/$MgAl_2O_4$	11 wt% CeO_2	8.3	59	9
Ni/CeO_2–K/$MgAl_2O_4$	5 wt% CeO_2 5 wt% K	8.2	54	6

distinguished as the Ni particles are the dark/black particles. The particle size determined from the TEM analysis was 8 nm ± 2 nm, which is similar to the XRD results. The trends in Ni particle sizes obtained by XRD are confirmed by TEM.

The XRD-patterns for NiO/CeO_2, $NiO/Ce_{0.6}Zr_{0.4}O_2$, $NiO/MgAl_2O_4$, and $NiO/CeZrO_4/MgAl_2O_4$ can be seen in Fig. S.3a, S.3b, S.3c, and S.3d, respectively, in Supplementary Data. XRD-analysis of the different catalysts confirmed that the mixed oxide of Ce and Zr was $Ce_{0.6}Zr_{0.4}O_2$ and that the $MgAl_2O_4$ indeed had spinel structure and was not a mixture of MgO and Al_2O_3. On the $Ni/MgAl_2O_4$ catalysts, some formation of $NiAl_2O_4$ phase was observed. Addition of K and CeO_2 to $Ni/MgAl_2O_4$ could not be detected by the XRD-analysis, probably due to the low amount present on the catalysts or because they were present as amorphous species. The loading of CeO_2 corresponded to roughly one monolayer, while the potassium loading was chosen based on the optimal value of 8 wt% K found by Hu and Lu [54]. Their catalyst however had a surface area of 125 m^2/g, roughly twice the value of our catalyst, and thus we used about 4 wt% K to provide the same surface coverage of K. It corresponded to about two monolayers of K.

The addition of $CeZrO_4$ to $Ni/MgAl_2O_4$ could be detected by XRD and confirmed the presence of $CeZrO_4$. No formation of mixed oxides with Ce or Zr incorporated in to the $MgAl_2O_4$-phase was observed showing that these species were present as true promoters on the surface of $MgAl_2O_4$.

Temperature controlled reduction has been conducted for $Ni/MgAl_2O_4$, $Ni/CeZrO_4/MgAl_2O_4$, Ni/CeO_2, and $Ni/Ce_{0.6}Zr_{0.4}O_2$ and is discussed in Supplementary Data. The main findings were that reduction of Ni started around 300 °C for all of the supports and especially for the two $MgAl_2O_4$ samples reduction also occurred at 600–800 °C, which could correspond to the reduction of $NiAl_2O_4$.

3.2. *Effect of temperature*

The effect of temperature on conversion and product distribution in SR of ethanol was investigated for several Ni-based catalysts at temperatures between 400 and 700 °C and an S/C-ratio of 6. The conversion over all of the catalysts at each temperature level initially decreased with time and then reached a relatively stable conversion after approximately 1.5 h. The decrease in conversion was largest at 400 °C and 500 °C, which shows that severe deactivation due to carbon deposition or oxidation of Ni occurred at the lowest temperatures. The conversion as function of time at the four temperature levels during SR of ethanol over $Ni/CeZrO_4/MgAl_2O_4$ can be seen in Fig. 1, while the initial and pseudo steady state conversion for the other catalysts can be seen in Table S.2 in Supplementary Data. The conversion reported in the following is the pseudo steady state conversion, unless otherwise stated.

The effect of temperature on the product distribution in the SR of ethanol at temperatures between 400 and 700 °C and S/C = 6 is described in the Supplementary Data. The main findings are that the conversion and yield of H_2 increased with temperature and reached respectively full conversion and a yield of H_2 of 72–75% at 700 °C. The yield of hydrocarbons decreased with temperature and was close to zero at 700 °C while the formation of ethene had a maximum at 500 °C. The product distribution resembled the thermodynamical equilibrium and approached equilibrium with increasing temperature. Furthermore no significant influence of the carrier material on the product distribution was found.

The effect of W/F in the SR of ethanol over $Ni/MgAl_2O_4$ at 600 °C was also investigated and it showed that as W/F became smaller the offgas composition moved away from the thermodynamical equilibrium as expected (see Fig. S.7 in Supplementary Data).

3.3. *Effect of carrier material*

The conversion as function of temperature over four different Ni-based catalysts is shown in Fig. 2. The conversion was highest for $Ni/Ce_{0.6}Zr_{0.4}O_2$ and $Ni/CeZrO_4/MgAl_2O_4$ while $Ni/MgAl_2O_4$ and Ni/CeO_2 had lower degrees of conversion. Similar differences were observed in initial activities (see Table S.2 in Supplementary Data).

The nickel particle size for the different catalysts ranged from 6 to 15 nm and it is generally assumed that smaller particles will be more active due to the higher dispersion and a higher number of active step sites [57]. However, the nickel particle size did not seem to be determining for the conversion as the $Ni/CeZrO_4/MgAl_2O_4$ and $Ni/MgAl_2O_4$, which had similar d_p (see Table 1), gave different conversions. Furthermore, $Ni/Ce_{0.6}Zr_{0.4}O_2$ with the largest nickel particles showed the highest conversion. Therefore it seems that the type of support is more important than the size of the nickel particles at least as long as the Ni particles do not differ much in size.

The high activity of $Ni/Ce_{0.6}Zr_{0.4}O_2$ could be ascribed to increased water dissociation for this support [10,58]. This will lead to more OH-species on the surface of the catalysts, which can react with C-species forming carbon oxides and H_2. Reactions with lattice oxygen on these types of support have also been proposed and might contribute as well [50]. Furthermore, it can be seen from Fig. 2 that the addition of CeO_2 and ZrO_2 to $MgAl_2O_4$ increased the conversion, which could be ascribed to a similar effect.

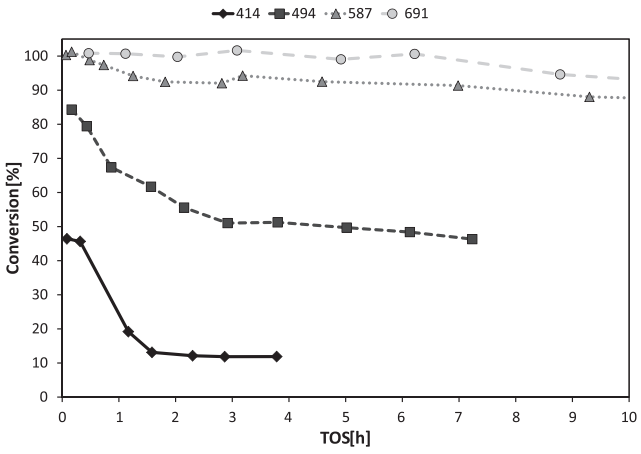

Fig. 1 – The conversion as function of time at the different temperatures over $Ni/CeZrO_4/MgAl_2O_4$. Experimental conditions: S/C: 5.8, m_{Cat} = 0.50 g, Ni loading: 8.2 wt%, F_T = 1.6 NL/min, y_{Eth} = 3.4 vol%, y_{H_2O} = 38.8 vol%, N_2 as balance.

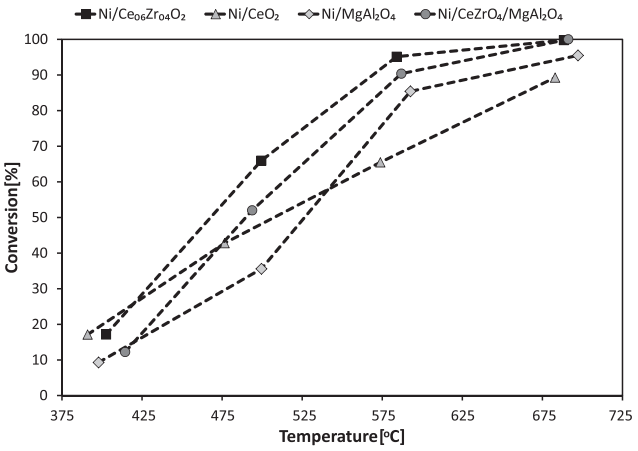

Fig. 2 – Comparison of conversion as function of temperature over the tested Ni-based catalysts. TOS: 50–70 h. Experimental conditions: S/C: 5.3–6.0, m_{Cat} = 0.50 g, Ni loading: 8.0–8.2 wt%, F_T = 1.5–1.6 NL/min, y_{Eth} = 3.2–3.5 vol%, y_{H_2O} = 38.6–39.2 vol%, N_2 as balance.

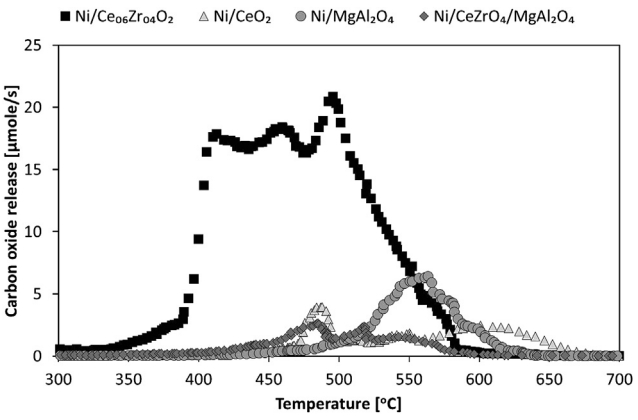

Fig. 4 – Carbon oxide release as function of temperature over Ni-based catalysts after 4 h on stream. Experimental conditions: F_T = 0.9–1 NL/min, O_2 = 2–3%, N_2 as balance, heating rate: 10 K/min.

3.3.1. *Deactivation*

It was chosen to test the different catalysts at approx. 600 °C for 4 h in order to determine differences in carbon deposition and activity during SR of ethanol. At this temperature full conversion was not achieved, which leads to a higher potential for forming carbon deposits and therefore it is easier to distinguish differences in catalytic performances.

The conversion as function of time over four different catalysts tested at 600 °C can be seen in Fig. 3. All the tested catalysts showed a more or less pronounced decrease in conversion with time. The deactivation was most pronounced for Ni/CeO_2 and $Ni/MgAl_2O_4$ while especially $Ni/Ce_{0.6}Zr_{0.4}O_2$ had a low drop in conversion with time.

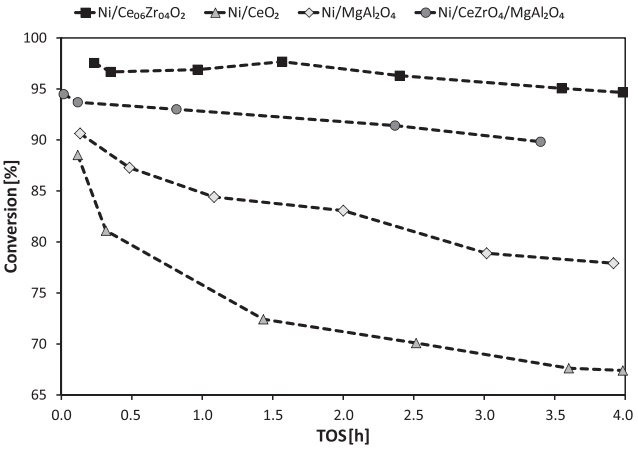

Fig. 3 – Conversion as function of time at 580 °C for Ni on four different supports. Experimental conditions: S/C: 5.3–6.0, Temp.: 579–585 °C, m_{Cat} = 0.50 g, Ni loading: 8.0–8.2 wt%, F_T = 1.5–1.6 NL/min, x_{Eth} = 3.2–3.5 vol%, y_{H_2O} = 38.6–39.2 vol%, N_2 as balance.

Deactivation in SR is often ascribed to sintering and carbon deposition [21,22]. TPO of the spent catalysts as well as measurement of surface area and nickel particle size of the spent catalysts were performed to elucidate what caused the deactivation.

The release of carbon oxides during TPO of the spent catalysts is shown in Fig. 4. It can be seen that the carbon oxides release occurred at different temperatures depending on the support material. $Ni/Ce_{0.6}Zr_{0.4}O_2$ showed carbon oxides release in a broad peak at temperatures between 350 and 580 °C. $Ni/MgAl_2O_4$ had a single broad peak with a maximum at 560 °C. Ni/CeO_2 had two peaks; one around 475 °C and a broad one from 550 °C to 650 °C. $Ni/CeZrO_4/MgAl_2O_4$ showed carbon oxides release at three different peak temperatures, 475 °C, 515 °C, and 545 °C. The first coincide with the first peak from Ni/CeO_2, while the last peak coincide with the oxidation from $Ni/MgAl_2O_4$. The results indicate that the coke was oxidized at different temperatures depending on whether it is located on a redox-active support or on the Ni particles. CeO_2 and $CeZrO_4$ are known as soot oxidation catalysts [52] and therefore these might catalyze the oxidation of carbon at lower temperature compared with $MgAl_2O_4$ and be responsible for the carbon release at temperatures below 550 °C.

The results from the TPO experiments can give an indication of which type of carbon was deposited on the catalysts. It has been reported that carbon oxides released below 500 °C arises from monoatomic carbon or filamentous carbon like single walled carbon nanotubes, while carbon released above 500 °C arises from amorphous carbon with different degrees of graphitization or bulkier forms of carbon nanotubes [35,59,60]. The oxidation agent in these studies was O_2. This could indicate that carbon formed on $Ni/Ce_{0.6}Zr_{0.4}O_2$ mainly was monoatomic carbon or single walled nanotubes, while the carbon formed on $Ni/MgAl_2O_4$ was amorphous carbon. On Ni/CeO_2 it appears that both types of carbon are formed as two peaks are observed. However due to the catalytic properties of CeO_2 and $CeZrO_4$ in carbon oxidation the above limits might not apply.

TEM-images of the spent catalysts were acquired to investigate this further. Fig. 5(a) and (b) shows TEM-images of

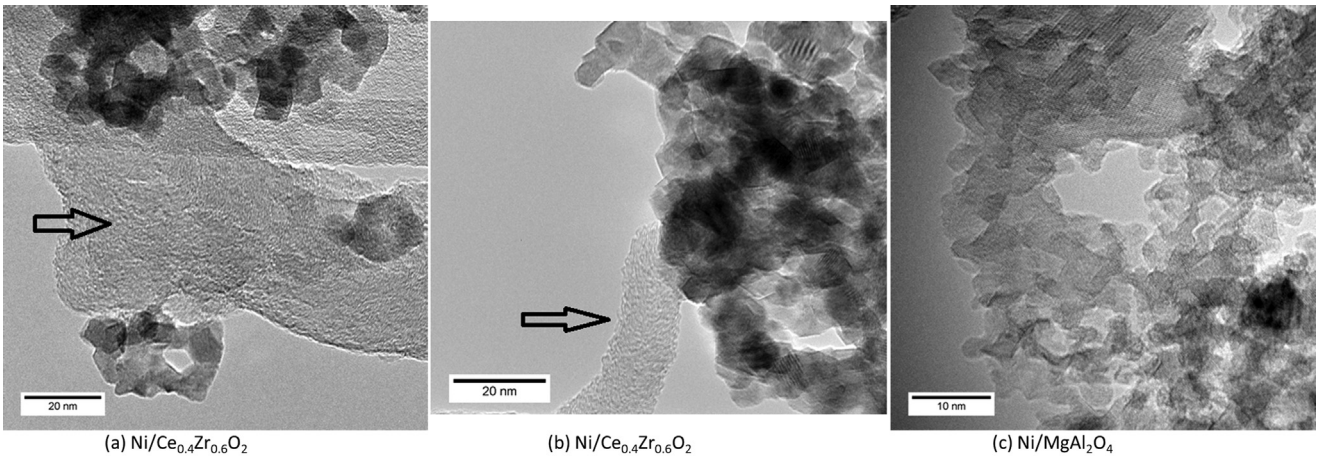

Fig. 5 – TEM-images of spent catalysts. Carbon whiskers in fig. (a) and (b) are indicated by an arrow.

spent $Ni/Ce_{0.6}Zr_{0.4}O_2$ particles and carbon whiskers can clearly be observed. This can, to some extent, explain the stable activity of this catalyst as the Ni particles will be able to catalyze the SR reactions despite carbon deposition [61,62]. A TEM image of a spent $Ni/MgAl_2O_4$ catalyst can be seen in Fig. 5(c). Analysis of this image and other images did not reveal carbon whiskers, which could indicate that the carbon was mainly present as encapsulating carbon.

The amount of carbon formed on each of the catalysts is shown in Table 2. $Ni/Ce_{0.6}Zr_{0.4}O_2$ had the highest carbon deposition, 15.2 mmole C/mole C_{Feed} or 96 mg C/(g_{Cat} × h), which may seem contradictory to the fact that it remained stable and active over time. However, as discussed above carbon was present as whiskers on this catalyst, which is known not to decrease the catalytic activity [61,62]. The other catalysts had much lower levels of carbon deposition in the range of 2–4 mmole C/mole C_{Feed} or 15–26 mg C/(g_{Cat} × h). The results show that adding to $CeZrO_4$ to $Ni/MgAl_2O_4$ decreased carbon deposition from 26 to 15 mg C/(g_{Cat} × h). This decrease could be due to reaction of coke with lattice oxygen from $CeZrO_4$ [52] or due to an increased amount of OH-species on the support. The carbon on $Ni/CeZrO_4/MgAl_2O_4$ was oxidized at a lower temperature compared with $Ni/MgAl_2O_4$, see Fig. 4, which shows that $CeZrO_4$ catalyzes carbon oxidation in the TPO experiments and will probably also do this under reaction conditions. Ni/CeO_2, $Ni/MgAl_2O_4$, and $Ni/CeZrO_4/MgAl_2O_4$ had nickel particles with a size of 6–10 nm while $Ni/Ce_{0.6}Zr_{0.4}O_2$ had nickel particles with d_p of 15–20 nm (see Table 1). Therefore the lower amount of carbon on Ni/CeO_2, $Ni/MgAl_2O_4$, and $Ni/CeZrO_4/MgAl_2O_4$ compared with $Ni/Ce_{0.6}Zr_{0.4}O_2$ could be due to smaller Ni particles, which lowers the risk of formation of carbon whiskers [53].

The BET surface area and XRD Ni particle size before and after a temperature dependence experiment are shown in Table 2. The surface area for Ni/CeO_2 and $Ni/Ce_{0.6}Zr_{0.4}O_2$ decreased by a factor of roughly 3 and 2, respectively, while the Ni particle size increased by a factor of 3 and 2. For $Ni/MgAl_2O_4$ and $Ni/CeZrO_4/MgAl_2O_4$ the surface area did not decrease significantly, while the Ni particle size increased by a factor of 1.5 for both catalysts. The change in Ni particle size for all the catalysts showed that sintering did occur. However, the two spinel based catalysts seemed more stable as the BET surface areas and Ni particle size did not change much over a 60–70 h experiment.

The results show that all the tested Ni-based catalysts suffer from sintering and carbon deposition to some extent, which led to deactivation. Therefore process based optimization is needed in order to minimize these problems.

3.4. *Effect of temperature on carbon deposition*

The carbon deposition and ethene formation as function of temperature in SR of ethanol at S/C = 6 over $Ni/MgAl_2O_4$ and $Ni/Ce_{0.6}Zr_{0.4}O_2$ can be seen in Fig. 6 for experiments with 4 h

Table 2 – Carbon deposition during a 4 h experiment at approx. 600 °C and BET surface area and XRD Ni particle size before and after a temperature dependence experiment with 60–70 h on stream. Experimental conditions: S/C: 5.3–6.0, Temp.: 579–585 °C, m_{Cat} = 0.50 g, Ni loading: 8.0–8.2 wt%, F_T = 1.5–1.6 NL/min, x_{Eth} = 3.2–3.5%, x_{H_2O} = 38.6–39.2%, N_2 as balance.

Catalyst	Carbon deposition		Surface area		NiNiO particle size	
	[mmole C/mole C_{Feed}]	[mg C/(g_{Cat} × h)]	Fresh [m^2/g]	Spent [m^2/g]	Fresh [nm]	Spent [nm]
$Ni/Ce_{0.6}Zr_{0.4}O_2$	15.2	96	90	42	15–20	20–28
Ni/CeO_2	2.9	19	113	35	10	27
$Ni/MgAl_2O_4$	4.1	26	69	66	7	11
$Ni/CeZrO_4/MgAl_2O_4$	2.2	15	63	53	6	9

on stream. The experiments for $Ni/Ce_{0.6}Zr_{0.4}O_2$ at 400 °C and 500 °C were stopped after 2 h on stream due to excessive carbon build up causing a large pressure drop over the reactor.

The carbon deposition on both $Ni/MgAl_2O_4$ and $Ni/Ce_{0.6}Zr_{0.4}O_2$ had a maximum at 500 °C. For $Ni/MgAl_2O_4$ it decreased with temperature from 15 mmole C/mole C_{Feed} to 0.03 mmole C/mole C_{Feed} (94–0.2 mg C/(g_{Cat} × h)) when increasing the temperature from 506 to 741 °C. For $Ni/Ce_{0.6}Zr_{0.4}O_2$ a significant decrease from 88 mmole C/mole C_{Feed} to 0.06 mmole C/mole C_{Feed} (552–0.4 mg C/(g_{Cat} × h)) in carbon deposition was observed when increasing the temperature from 495 to 755 °C. The peak release of carbon oxides over $Ni/MgAl_2O_4$ during TPO occurred at 520 °C after operating at 400 °C while carbon oxides release after operating at 700 °C occurred at 600 °C. For $Ni/Ce_{0.6}Zr_{0.4}O_2$ an additional carbon oxides release peak at 630 °C was observed after operation at 700 °C and 750 °C. The shift in carbon oxide release towards higher temperatures during TPO indicated that the carbon deposited at low temperatures had a lower degree of graphitization and was more reactive.

The formation of ethene as function of temperature, see Fig. 6, had a maximum at 500 °C and at low temperatures were significantly higher for $Ni/Ce_{0.6}Zr_{0.4}O_2$ compared to $Ni/MgAl_2O_4$. The maximum in carbon deposition over both catalysts coincide with the maximum of ethene in the offgas, which is a very potent coke precursor [63,64]. This could explain the high deposition of carbon at 500 °C. Thermodynamic analysis using the measured and thermodynamic equilibrium offgas composition (Rostrup–Nielsen and Christiansen [47]) did not show potential for carbon formation from methane decomposition, Boudouard reaction, or CO decomposition.

The decrease in carbon deposition with increasing temperature could also be explained by an increased reaction rate

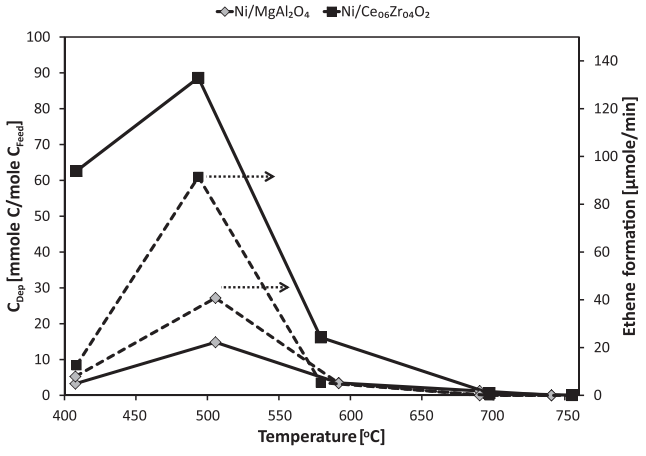

Fig. 6 – Carbon deposition and ethene formation after 4 h on stream as function of temperature over $Ni/MgAl_2O_4$ and $Ni/Ce_{0.6}Zr_{0.4}O_2$. Full lines: Carbon deposition; Dashed lines: Ethene formation. The experiments at 400 and 500 °C for $Ni/Ce_{0.6}Zr_{0.4}O_2$ were stopped after 2 h due to risk of blockage. Experimental conditions: S/C: 5.5–6.2, Temp: 408–755 °C, m_{Cat} = 0.50 g, Ni loading: 8.1–8.2 wt%, F_T = 1.5 NL/min, y_{Eth} = 3.2–3.6 vol%, y_{H_2O} = 38.8–39.0 vol%, N_2 as balance.

for the SR reactions leading to fewer carbon species on the surface of the catalysts. Furthermore the gasification of deposited carbon by either steam or CO_2 will increase with temperature as well. At the lowest temperature of 400 °C ethanol is not activated and therefore conversion and carbon deposition are lower. As shown in Fig. 1, there was a large drop in conversion at 400 °C over time, even larger than at 500 °C, where carbon deposition was more severe. An explanation could be partial oxidation of the catalyst at 400 °C caused by the high amounts of steam present and the low concentration of H_2.

Results from thermodynamic and experimental studies of the SR of ethanol in the literature predict a decrease in carbon deposition with temperature [65–69]. Similar to this study, Wang et al. [70] found a maximum in carbon deposition at 500 °C for SR of ethanol over a Co/CeO_2 catalyst. Wang et al. [70] ascribed the high carbon formation to disproportionation of CO and CH_4 and a slow reaction rate for steam and dry reforming. Another and perhaps more likely explanation could be a formation of carbon from ethene, as indicated in Fig. 6.

An interesting difference between $Ni/MgAl_2O_4$ and $Ni/Ce_{0.6}Zr_{0.4}O_2$ was found in the product distribution at 750 °C where $Ni/MgAl_2O_4$ completely converted ethanol to carbon oxides while $Ni/Ce_{0.6}Zr_{0.4}O_2$ still had small amounts of methane in the offgas even at 755 °C. Furthermore, a slight loss in both methane SR and WGS activity with time over $Ni/Ce_{0.6}Zr_{0.4}O_2$ was observed at 755 °C, whereas $Ni/MgAl_2O_4$ was stable over time (the experiment had a run time of 4 h).

A drawback of running at high temperatures is that sintering is more likely to occur. Therefore the surface area of the spent catalysts was measured to investigate how severe the sintering was and the results are shown in Table 3. It can be seen that no sintering of the catalysts took place at temperatures between 500 °C and 700 °C, while at approx. 750 °C sintering increased and the surface area decreased.

3.5. *Effect of additives to $Ni/MgAl_2O_4$ catalysts*

Steam reforming of ethanol at 600 °C for 4 h and subsequent determination of carbon deposition was conducted for $Ni/MgAl_2O_4$ promoted with K, CeO_2, ZrO_2, or mixtures hereof to evaluate whether these additives could have a beneficial effect on the catalyst performance. The BET surface area, Ni particle size, additive- and Ni loading for the promoted catalysts can be seen in Table 1. The additives did not significantly influence Ni particle size or surface area and therefore the changes in catalytic performance can be ascribed to the properties of the additives.

The conversion as function of time for the different $Ni/MgAl_2O_4$ catalysts can be seen in Fig. 7. The conversion was high and relatively stable for the catalysts promoted with K, CeO_2–K, $CeZrO_4$, and $K/CeZrO_4$. The base catalyst behaved as shown previously and showed a decrease in conversion over the entire 4 h while the catalyst with CeO_2 had an induction period of 1 h before reaching a stable conversion in the range of 85%. In conclusion adding CeO_2, K, or $CeZrO_4$ seem to promote a more stable performance of the catalyst.

The product distributions were similar for the unpromoted and promoted $Ni/MgAl_2O_4$ and above 95% of the converted

Table 3 – Surface area (m^2/g) of $Ni/Ce_{0.6}Zr_{0.4}O_2$ and $Ni/MgAl_2O_4$ after 4 h on stream at different temperatures. Experimental conditions: S/C: 5.5–6.2, Temp: 408–755 °C, m_{Cat} = 0.50 g, Ni loading: 8.1–8.2 wt%, F_T = 1.5 NL/min, y_{Eth} = 3.2–3.6 vol%, y_{H_2O} = 38.8–39.0 vol%, N_2 as balance.

Catalyst	Fresh	400 °C	500 °C	600 °C	700 °C	750 °C
$Ni/Ce_{0.6}Zr_{0.4}O_2$	88	–	–	67	67	53
$Ni/MgAl_2O_4$	69	66	61	61	60	53

ethanol formed carbon oxides, hydrogen, and small amounts of methane and ethene (less than 5% yield of C_xH_y). However, a slight increase in CH_4 production was observed for the promoted catalysts compared with $Ni/MgAl_2O_4$. The formation of ethene was similar for the base case and most of the promoted catalysts. Two exceptions were for $Ni/K–CeO_2/MgAl_2O_4$ which had no ethene in the offgas, and $Ni/CeO_2/MgAl_2O_4$, which had a higher yield of ethene. The decrease in carbon deposition was not due to changes in ethene formation and therefore it appears the role of the additives is to increase the rate of SR reactions and hereby minimize the carbon deposition.

The effect of tested additives on conversion, yield of ethene, and carbon deposition are shown in Fig. 8. All of the additives improved the catalyst performance either with respect to conversion, carbon deposition, or in most of the cases both. Promotion with CeO_2 led to the lowest carbon deposition of 0.9 mmole C/mole C_{Feed} or 6 mg C/(g_{Cat} × h) while the conversion was similar to the base case. Ni/CeO_2 had the lowest activity of the four tested support materials and sintered quite significantly, however it did show low carbon deposition. The higher conversion of ethanol over $Ni–CeO_2/MgAl_2O_4$ compared to Ni/CeO_2, as well as an improved stability could be explained by a stabilization of the CeO_2 on $MgAl_2O_4$ so sintering decreased (see Figs. 3 and 7). The decrease in carbon deposition might be explained by ceria monomers or small CeO_2 particles on $MgAl_2O_4$, which facilitated oxidation of surface carbon during SR.

$Ni–K/MgAl_2O_4$ also showed a decrease in carbon deposition and as well as an increased conversion compared with the base case. Therefore K and CeO_2 both seem to influence the catalyst by enhancing oxidation/gasification or decreasing deposition of solid carbon while K also induces a higher activity. Similar trends have been reported by others [19,54]. Adding both CeO_2 and K to the base catalyst improved the conversion while carbon deposition was on a level between adding either only K or only CeO_2. The promotion with $CeZrO_4$ also increased conversion, but carbon deposition was the highest among the promoted catalysts, albeit still significantly lower than the base $Ni/MgAl_2O_4$ catalyst. The increase in conversion when adding $CeZrO_4$ could be due to increased water dissociation, as mentioned earlier. The $Ni/K–CeO_2/MgAl_2O_4$ seems to be the most interesting catalyst as it showed high conversion combined with a low carbon deposition.

$Ni/K–CeO_2/MgAl_2O_4$ and $Ni–K/CeZrO_4/MgAl_2O_4$ both showed almost full conversion and to ensure that the low carbon deposition was due to the additives and not full conversion the experiments were repeated at a higher space velocity. The results from the experiments at different space velocities are shown in Table 4. The results show interestingly that the same amount of carbon was deposited at the higher space velocity with conversion around 80% and this shows that the additives do decrease the carbon deposition in the case of $Ni/K–CeO_2/MgAl_2O_4$ and $Ni–K/CeZrO_4/MgAl_2O_4$ also under more demanding conditions. The yield of ethene increased slightly with increasing space velocity, however it did not seem to influence the carbon deposition significantly. The carbon deposition seemed to be more dependent on temperature compared to space velocity as the increasing the space velocity did not influence the total carbon deposition.

Carbon burn-off experiments were also carried for the $Ni/MgAl_2O_4$ catalysts with the different additives. The carbon release as function of temperature is shown in Fig. S.8 in Supplementary Data. The carbon release peak for the

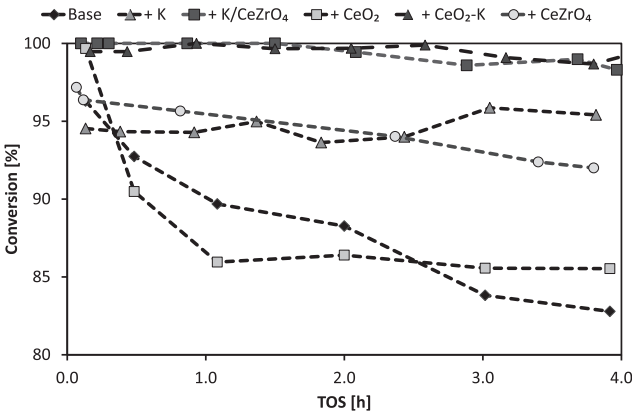

Fig. 7 – Conversion as function of time on stream for $Ni/MgAl_2O_4$ with different additives. Experimental conditions: S/C: 5.6–6.1, Temp.: 579–592 °C, m_{Cat} = 0.50 g, Ni loading: 8.0–8.3 wt%, F_T = 1.5 NL/min, y_{Eth} = 3.2–3.6 vol%, y_{H_2O} = 38.8–39.0 vol%, N_2 as balance.

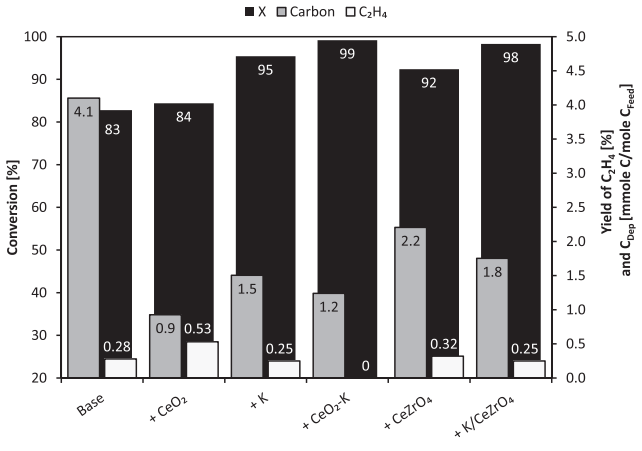

Fig. 8 – Comparison of conversion, carbon deposition, and yield of ethene after 4 h on stream for $Ni/MgAl_2O_4$ catalysts with different additives. Experimental conditions: S/C: 5.6–6.1, Temp.: 579–592 °C, m_{Cat} = 0.50 g, Ni loading: 8.0–8.3 wt%, F_T = 1.5 NL/min, y_{Eth} = 3.2–3.6 vol%, y_{H_2O} = 38.8–39.0 vol%, N_2 as balance.

Table 4 – Conversion and carbon deposition in SR of ethanol after 4 h on stream over Ni/K–CeO_2/$MgAl_2O_4$ and Ni–K/$CeZrO_4$/$MgAl_2O_4$ at different space velocities. Experimental conditions: S/C: 5.6–6.1, Temp.: 579–592 °C, m_{Cat} = 0.264–0.50 g, Ni loading: 8.2 wt%, F_T = 1.5 NL/min, y_{Eth} = 3.2–3.5 vol%, y_{H_2O} = 38.8–39.0 vol%, N_2 as balance.

Catalyst	WHSV [h^{-1}]	Conversion [%]	Carbon deposition		$Y_{C_2H_4}$ [%]
			[mmole C/mole C_{Feed}]	[mg C/h]	
Ni/K–CeO_2	13	98	1.2	4	0.00
Ni/K–CeO_2	25	81	1.3	4	0.28
Ni–K/$CeZrO_4$	12	100	1.8	5	0.24
Ni–K/$CeZrO_4$	25	81	1.5	5	0.59

promoted catalysts shifted towards lower temperatures, which indicates that combustion and also gasification is catalyzed by K as well as ZrO_2 and CeO_2. However, the difference could also be due to different types of carbon on the catalysts. The catalyzing effects of K, CeO_2, and ZrO_2 on combustion and gasification is known from the combustion and gasification literature [52,71,72]. This is also a contributing factor to the lowering of carbon deposition as well as the increase in activity observed in this study.

3.5.1. *Effect of TOS*

Two of the catalysts with additives, which showed a rather stable conversion with time and a low deposition of carbon, were tested for an extended period of time (24 h) to further investigate stability and carbon deposition. The conversion and yield of hydrocarbons as function of time for Ni–K/$MgAl_2O_4$ and Ni/CeO_2–K/$MgAl_2O_4$ can be seen in Fig. 9. The conversion over both catalysts decreased slowly with time with a rate of roughly 0.1 %-point pr. h. Furthermore the yield of hydrocarbons increased with time and a more pronounced increase was observed after 20 h on stream. No ethene was detected in the effluent from SR of ethanol over Ni/CeO_2–K/$MgAl_2O_4$, while the yield of ethene increased from 0.10% to

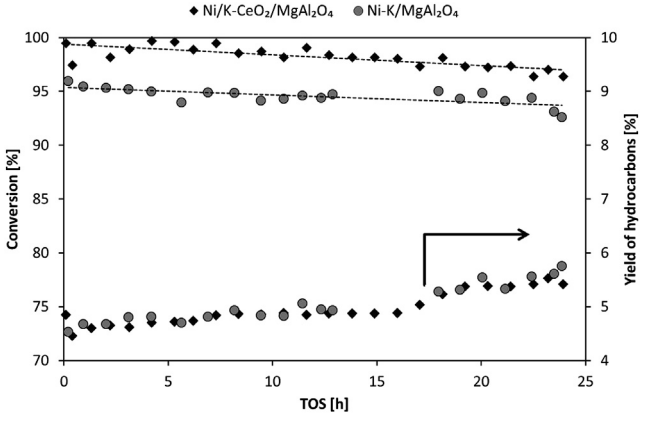

Fig. 9 – Conversion and yield of hydrocarbons as function of time for Ni–K/$MgAl_2O_4$ and Ni/CeO_2–K/$MgAl_2O_4$. Experimental conditions: S/C: 6, Temp.: 576 °C, m_{Cat} = 0.50 g, Ni loading: 8.0–8.3 wt%, F_T = 1.5 NL/min, y_{Eth} = 3.3 vol%, y_{H_2O} = 40.1 vol%, N_2 as balance.

Table 5 – Total carbon deposition and average rate of formation on Ni–K/$MgAl_2O_4$ and Ni/CeO_2–K/$MgAl_2O_4$ as function of time at 600 °C. Average values are from intervals from 0 to 4 h and 4–24 h. Experimental conditions: S/C: 6.0, Temp: 579–586 °C, m_{Cat} = 0.50 g, Ni loading: 8.2 wt%, F_T = 1.5–1.6 NL/min, y_{Eth} = 3.7–3.9 vol %, y_{H_2O} = 38.9 vol%, N_2 as balance.

Catalyst	Time [h]	Total C_{Dep} [mg C]	Average rate of C_{Dep} [mg C/h]
Ni–K/$MgAl_2O_4$	4	20	4.9
Ni–K/$MgAl_2O_4$	24	44	1.2
Ni/CeO_2–K/$MgAl_2O_4$	4	17	4.2
Ni/CeO_2–K/$MgAl_2O_4$	24	33	0.8

0.16% over Ni–K/$MgAl_2O_4$. Therefore deactivation was apparent even though the first 4 h on stream appeared stable. However the decrease in conversion with time was more pronounced for Ni/$MgAl_2O_4$ and therefore the additives still provided a marked improvement.

The amount of carbon formed after 24 h on stream was determined and the total carbon deposition and the average rate of carbon formation at different times can be seen in Table 5. The carbon deposition over Ni–K/$MgAl_2O_4$ and Ni/CeO_2–K/$MgAl_2O_4$ was quite similar after 4 h, however the buildup of carbon after 24 h was lower for Ni/CeO_2–K/$MgAl_2O_4$. This could indicate that CeO_2 has a positive effect on the carbon deposition even during longer periods of operation.

TEM-images of spent Ni–K/$MgAl_2O_4$ and Ni/CeO_2–K/$MgAl_2O_4$ can be seen in Fig. S.9 in Supplementary Data. These images show that carbon whiskers were formed on both catalysts. Carbon whiskers can, with time, break the catalyst pellets causing pressure drop over the catalyst bed, which can be detrimental for industrial units, due to mal distribution of the gas causing local hot spots [47].

The surface area and nickel particle size before and after a 24 h experiment at 600 °C can be seen in Table 6. The surface area of the catalysts did not change during 24 h operation at 600 °C. However the Ni particle size increased from 7 to 12 nm for Ni–K/$MgAl_2O_4$ and from 6 to 9 nm for Ni/CeO_2–K/$MgAl_2O_4$, which indicate sintering of the Ni particles for both of the catalysts.

3.6. *Sulfur addition*

Sulfur addition was investigated on Ni–CeO_2/$MgAl_2O_4$ to test if coverage of part of the Ni particles by sulfur could decrease

Table 6 – Comparison between BET surface area and XRD Ni particle size for Ni–K/$MgAl_2O_4$ and Ni/CeO_2–K/$MgAl_2O_4$ before and after a stability experiment with 24 h on stream at 600 °C.

Catalyst	Surface area		Ni particle size	
	Fresh [m^2/g]	Spent [m^2/g]	Fresh [nm]	Spent [nm]
Ni–K/$MgAl_2O_4$	55	55	7	12
Ni/CeO_2–K/$MgAl_2O_4$	54	54	6	9

Table 7 – Conversion, H_2-yield, hydrocarbon yield, and carbon deposition for $Ni/CeO_2/MgAl_2O_4$ at different degrees of sulfur coverage and with different sulfur sources. Sulfur added as K_2SO_4 or as H_2SO_4. TOS: 4 h. Experimental conditions: S/C: 5.7–6.0, Temp: 586–588 °C, m_{Cat} = 0.50 g, Ni loading: 8.1–8.2 wt%, F_T = 1.5 NL/min, y_{Eth} = 3.3–3.4 vol%, y_{H_2O} = 38.8–39.0 vol%, N_2 as balance.

Sulfur [wt% S]	Agent	S-coverage [%]	Conversion [%]	Carbon deposition		Y_{H_2} [%]	Y_{CyHx} [%]
				[mg C/(g_{Cat} × h)]	[mmole C/mole C_{Feed}]		
0		0	85	6.0	0.93	80	3.5
0.03	K_2SO_4	6	90	1.2	0.15	74	6.2
0.06	K_2SO_4	13	89	2.2	0.34	73	9.5
0.06	H_2SO_4	13	85	3.3	0.51	63	11.6
0.12	K_2SO_4	26	89	2.4	0.34	64	12.7

the carbon deposition. Sulfur is expected to cover the step sites which are active in carbon deposition and hereby decrease the formation of solid carbon or the presence of sulfur might limit the size of carbon islands and inhibit the formation of carbon whiskers [47,62]. A sulfur coverage of approx. 13% (0.06 wt% S) on $Ni–CeO_2/MgAl_2O_4$ was achieved by impregnation with an aqueous solution of K_2SO_4 or H_2SO_4 to test if a decrease in carbon deposition could be achieved and how the conversion and product distribution would be influenced by sulfur, or sulfur and potassium. The sulfur and potassium content of fresh and spent catalysts was determined by ICP-OES and the results were close to the expected level as shown in Supplementary Data. Thus neither sulfur nor potassium were lost from the catalyst during calcination or reduction.

The conversion, yield of hydrocarbons, and carbon deposition with and without sulfur are presented in Table 7. An increase in conversion and hydrocarbon selectivity, and a decrease in carbon deposition upon sulfur addition by K_2SO_4 was observed. The increase in conversion was unexpected as sulfur is known to inhibit SR due to blockage of surface sites on the Ni species. Therefore the effect of K was investigated by adding the sulfur in the form of H_2SO_4. Potassium can influence the catalytic performance and increase conversion as shown in section 3.5 in this work as well as by others [19,54]. Table 7 shows that impregnation with H_2SO_4 induced a decrease in carbon deposition and a larger increase in yield of hydrocarbons compared with K_2SO_4, but the conversion was similar to the base case. Therefore, the increased conversion might be ascribed to the presence of potassium and it also appears that K induces a lower hydrocarbon yield. This was also reported by Hu and Lu [54], who investigated the effect of potassium on Ni/Al_2O_3 in the SR of acetic acid. The increase in the yield of hydrocarbons compared with the base catalyst can be interpreted as a decrease in activity as the hydrocarbons were not converted to the same extent. The hydrocarbons were 95% CH_4 and the rest was ethene. Interestingly, the amount of ethene formed was highest with sulfur present so the decrease in carbon deposition cannot be ascribed to a decrease in the ethene formation.

The catalysts impregnated with either H_2SO_4 or K_2SO_4 showed quite stable conversion and product distribution with time on stream. A slight increase in the yield of ethene with time was observed $Ni–CeO_2/MgAl_2O_4$ impregnated with H_2SO_4. The product yields and conversion as function of time over $Ni–CeO_2/MgAl_2O_4$ impregnated with 0.06 wt% S by either H_2SO_4 or K_2SO_4 as impregnation agent can be seen in Fig. S.10a and S.10b in Supplementary Data.

Catalysts with a sulfur loading of 0.03 wt%, 0.06 wt%, and 0.12 wt% were synthesized by impregnation with K_2SO_4 to investigate the influence of the amount of sulfur on the catalytic performance and the results of these tests are shown in Table 7. It was found that the hydrocarbon yield increased while the H_2-yield decreased with increasing amounts of sulfur on the catalysts. All of the sulfur treated catalysts showed a relatively stable conversion during the 4-h experiments. This shows that sulfur does inhibit especially conversion of methane and ethene to carbon oxides and H_2. The carbon deposition is lower with sulfur than without in the three cases investigated with a minimum at 6% sulfur coverage. These results indicate that addition of small amounts of sulfur can be used to block sites on the catalyst and hereby inhibit carbon deposition. The loss in activity due to sulfur can mainly be seen as an increase in the yield of hydrocarbons. Bengaard et al. [57] have shown that the SR of CH_4 has a lower energy barrier on step sites and blockage of these sites will lead to a lower conversion of methane. This entails a lower amount of carbon species on the surface and a lower risk of carbon deposition due to slower nucleation of carbon whiskers or agglomeration of carbon deposits.

4. Conclusions

In this work the SR of ethanol was investigated over Ni-based catalysts and several strategies for minimizing carbon deposition by changing the catalyst formulation were explored. The main conclusions are:

- Carbon deposition and sintering leading to loss af activity was apparent in SR of ethanol for Ni supported on different carriers including CeO_2, $Ce_{0.6}Zr_{0.4}O_2$, $MgAl_2O_4$, and $CeZrO_4/MgAl_2O_4$.
- Carbon deposition was most severe at 500 °C most likely due to a high fraction of ethene in the product gas which is a known as a severe carbon precursor. Increasing the temperature to 700 °C or above significantly decreased the carbon deposition.
- Promotion of $Ni/MgAl_2O_4$ with K, CeO_2, and ZrO_2 increased the conversion and lowered the carbon deposition by factors of 2–4. These catalysts appeared very stable over 4 h of operation. Potassium most likely

partly blocks the sites of carbon formation, while the redox-active promoters increase the OH availability on the catalyst and/or provide lattice oxygen for reaction with carbon precursors.

- Experiments over 24 h with $Ni/CeO_2–K/MgAl_2O_4$ and $Ni–K/MgAl_2O_4$ catalysts, however, did show a slow decrease in activity with time accompanied with carbon deposition with a rate of 0.8–1.2 mg C/h. The carbon formed after 24 h was partly as carbon whiskers, which can be detrimental for SR reactors.
- Selective poisoning with sulfur in the form of SO_4 to $Ni–CeO_2/MgAl_2O_4$ led to a decrease in carbon deposition as well as the overall activity of the catalyst, probably due to blockage of step sites on the Ni particles. The lowest carbon deposition rate over 4 h of operation of all the tested catalysts was obtained for the $Ni–CeO_2/MgAl_2O_4$ catalyst with 0.03 wt% S added in the form of K_2SO_4.

The results show that it is possible to improve the stability and activity of Ni-based catalysts in steam reforming of oxygenated species by suitable promoters. Nevertheless carbon formation still takes place which indicates that other, process related means are needed as well for long term operation.

Acknowledgments

This work is part of the CHEC (Combustion and Harmful Emission Control) Research Center, EGSSE (European Graduate School of Sustainable Energy), and CASE (Catalysis for Sustainable Energy). The present work is financed by The Technical University of Denmark. Zoltam Imre Balogh and Thomas Willum Hansen from the DTU CEN and Irek Sharafutdinov from DTU Physics are gratefully acknowledged for assistance with, respectively, TEM and TPR-measurements. Furthermore, Haldor Topsoe are acknowledged for help with the elemental analysis of the catalysts.

Appendix A. Supplementary data

Supplementary data related to this article can be found at http://dx.doi.org/10.1016/j.ijhydene.2013.09.027.

REFERENCES

[1] Raffelt K, Henrich E, Koegel A, Stahl R, Steinhardt J, Weirich F. The BTL2 process of biomass utilization entrained-flow gasification of pyrolyzed biomass slurries. Appl Biochem Biotechnol 2006;129:153–64.
[2] Venderbosch RH, Prins W. Fast pyrolysis technology development. Biofuel Bioprod Bioref 2010;4:178–208.
[3] Oasmaa A, Czernik S. Fuel oil quality of biomass pyrolysis oils- state of the art for the end users. Energy Fuels 1999;13:914–21.
[4] Oasmaa A, Meier D. Norms and standards for fast pyrolysis liquids 1. Round robin test. J Anal Appl Pyrolysis 2005;73:323–34.
[5] Demirbas A. Competitive liquid biofuels from biomass. Appl Energy 2011;88:17–28.
[6] Trane R, Jensen AD, Dahl S. Catalytic steam reforming of bio-oil. Int J Hydrogen Energy 2012;37:6447–72.
[7] Mortensen PM, Grunwaldt JD, Jensen PA, Knudsen KG, Jensen AD. A review of catalytic upgrading of bio-oil to engine fuel. Appl Catal A Gen 2011;407:1–19.
[8] Huber GW, Iborra S, Corma A. Synthesis of transportation fuels from biomass: chemistry, catalysts, and engineering. Chem Rev 2006;106:4044–98.
[9] Wang D, Czernik S, Montane D, Mann M, Chornet E. Biomass to hydrogen via fast pyrolysis and catalytic steam reforming of the pyrolysis oil or its fractions. Ind Eng Chem Res 1997;36:1507–18.
[10] Rioche R, Kulkarni S, Meunier FC, Breen JP, Burch R. Steam reforming of model compounds and fast pyrolysis bio-oil on supported noble metal catalysts. Appl Catal B Environ 2005;61:130–9.
[11] Basagiannis AC, Verykios XE. Steam reforming of the aqueous fraction of bio-oil over structured $Ru/MgO/Al_2O_3$ catalysts. Catal Today 2007;127:256–64.
[12] Czernik S, French R, Feik C, Chornet E. Hydrogen by catalytic steam reforming of liquid byproducts from biomass thermoconversion processes. Ind Eng Chem Res 2002;41:4209–15.
[13] Hou T, Yuan L, Ye T, Gong L, Tu J, Yamamoto M, et al. Hydrogen production by low-temperature reforming of organic compounds in bio-oil over a CNT-promoting Ni catalyst. Int J Hydrogen Energy 2009;34:9095–107.
[14] Yan CF, Cheng FF, Hu RR. Hydrogen production from catalytic steam reforming of bio-oil aqueous fraction over Ni/CeO_2-ZrO_2 catalysts. Int J Hydrogen Energy 2010;35:11693–9.
[15] Heracleous E. Well-to-wheels analysis of hydrogen production from bio-oil reforming for use in internal combustion engines. Int J Hydrogen Energy 2011;36:11501–11.
[16] Oasmaa A, Kuoppala E, Selin JF, Gust S, Solantausta Y. Fast pyrolysis of forestry residue and pine. 4. Improvement of the product quality by solvent addition. Energy Fuels 2004;18:1578–83.
[17] Bridgwater AV. Renewable fuels and chemicals by thermal processing of biomass. Chem Eng J 2003;91:87–102.
[18] Cavallaro S, Chiodo V, Freni S, Mondello N, Frusteri F. Performance of Rh/Al_2O_3 catalyst in the steam reforming of ethanol: H_2 production for MCFC. Appl Catal A Gen 2003;249:119–28.
[19] Rass-Hansen J, Christensen CH, Sehested J, Helveg S, Rostrup-Nielsen JR, Dahl S. Renewable hydrogen: carbon formation on Ni and Ru catalysts during ethanol steam-reforming. Green Chem 2007;9:1016–21.
[20] Galletti AE, Gomez MF, Arra LA, Abello MC. Ni catalysts supported on modified $ZnAl_2O_4$ for ethanol steam reforming. Appl Catal A Gen 2010;380:40–7.
[21] Ni M, Leung D, Leung M. A review on reforming bio-ethanol for hydrogen production. Int J Hydrogen Energy 2007;32:3238–47.
[22] Haryanto A, Fernando S, Murali N, Adhikari S. Current status of hydrogen production techniques by steam reforming of ethanol: a review. Energy Fuels 2005;19:2098–106.
[23] Cavallaro S, Chiodo V, Vita A, Freni S. Hydrogen production by auto-thermal reforming of ethanol on Rh/Al_2O_3 catalyst. J Power Sources 2003;123:10–6.
[24] Basagiannis AC, Panagiotopoulou P, Verykios XE. Low temperature steam reforming of ethanol over supported noble metal catalysts. Top Catal 2008;51:2–12.
[25] Fatsikostas AN, Verykios XE. Reaction network of steam reforming of ethanol over Ni-based catalysts. J Catal 2004;225:439–52.
[26] De Rogatis L, Montini T, Lorenzut B, Fornasiero P. $Ni_x Cu_y/Al_2O_3$ based catalysts for hydrogen production. Energy Environ Sci 2008;1:501–9.

[27] Hung CC, Chen SL, Liao YK, Chen CH, Wang JH. Oxidative steam reforming of ethanol for hydrogen production on M/Al_2O_3. Int J Hydrogen Energy 2012;37:4955–66.
[28] Liguras DK, Kondarides DI, Verykios XE. Production of hydrogen for fuel cells by steam reforming of ethanol over supported noble metal catalysts. Appl Catal B Environ 2003;43:345–54.
[29] Palmeri N, Chiodo V, Freni S, Frusteri F, Bart JCJ, Cavallaro S. Hydrogen from oxygenated solvents by steam reforming on Ni/Al_2O_3 catalyst. Int J Hydrogen Energy 2008;33:6627–34.
[30] Le Valant A, Can F, Bion N, Duprez D, Epron F. Hydrogen production from raw bioethanol steam reforming: optimization of catalyst composition with improved stability against various impurities. Int J Hydrogen Energy 2010;35:5015–20.
[31] Moura JS, Souza MOG, Bellido JDA, Assaf EM, Opportus M, Rangel MC, et al. Ethanol steam reforming over rhodium and cobalt-based catalysts: effect of the support. Int J Hydrogen Energy 2012;37:3213–24.
[32] Rass-Hansen J, Johansson R, Møller M, Christensen CH. Steam reforming of technical bioethanol for hydrogen production. Int J Hydrogen Energy 2008;33:4547–54.
[33] Ciambelli P, Palma V, Ruggeiro A. Low temperature catalytic steam reforming of ethanol. 2. Preliminary kinetic investigation of Pt/CeO_2 catalysts. Appl Catal B Environ 2010;96:190–7.
[34] Diagne C, Idriss H, Pearson K, Gomez-Garcia MA, Kiennemann A. Efficient hydrogen production by ethanol reforming over Rh catalysts. Effect of addition of Zr on CeO_2 for the oxidation of CO to CO_2. C R Chim 2004;7:617–22.
[35] Padilla R, Benito M, Rodrigues L, Muñoz G, Daza L. Nickel and cobalt as active phase on supported zirconia catalysts for bio-ethanol reforming: influence of the reaction mechanism on catalysts performance. Int J Hydrogen Energy 2010;35:8921–8.
[36] Zhang B, Tang X, Li Y, Cai W, Xu Y, Shen W. Steam reforming of bio-ethanol for the production of hydrogen over ceria-supported Co, Ir and Ni catalysts. Catal Commun 2006;7:367–72.
[37] Cai W, Wang F, Daniel C, van Veen AC, Provendier H, Mirodatos C. Oxidative steam reforming of ethanol over Ir/CeO_2 catalysts: a structure sensitivity analysis. J Catal 2012;286:137–52.
[38] da Silva AM, de Souza KR, Jacobs G, Graham UM, Davis BH, Noronha FB, et al. Steam and CO_2 reforming of ethanol over Rh/CeO_2 catalyst. Appl Catal B Environ 2011;102:94–109.
[39] de Lima SM, Silva AM, da Cruz IO, Jacobs G, Davis BH, Noronha FB, et al. H_2 production through steam reforming of ethanol over Pt/ZrO_2, Pt/CeO_2 and Pt/$CeZrO_2$ catalysts. Catal Today 2008;138:162–8.
[40] Peela NR, Mubayi A, Kunzru D. Steam reforming of ethanol over Rh/CeO_2/Al_2O_3 catalysts in a microchannel reactor. Chem Eng J 2011;167:578–87.
[41] Jalowiecki-Duhamel L, Pirez C, Capron M, Dumeignil F, Payen E. Hydrogen production from ethanol steam reforming over cerium and nickel based oxyhydrides. Int J Hydrogen Energy 2010;35:12741–50.
[42] Zhou G, Barrio L, Agnoli S, Senanayake SD, Evans J, Rodriguez JA, et al. High activity of Ce_{1-x} Ni_x O_{2-y} for H_2 production through ethanol steam reforming: tuning catalytic performance through metal-oxide interactions. Angew Chem Int Ed 2010;49:9680–4.
[43] de Lima SM, da Silva AM, de Costa LO, Assaf JM, Mattos LV, Noronha FB, et al. Hydrogen production through oxidative steam reforming of ethanol over Ni-based catalysts derived from $La_{1-x}Ce_xNiO_3$ perovskite-type oxides. Appl Catal B Environ 2012;121:1–9.
[44] Barattini L, Ramis G, Resini C, Busca G, Sisani M, Constantino U. Reaction path of ethanol and acetic acid steam reforming over Ni–Zn–Al catalysts. Flow reactor studies. Chem Eng J 2009;153:43–9.
[45] Subramani V, Song C. Advances in catalysis and processes for hydrogen production from ethanol reforming. Cat 2007;20:65–106.
[46] Vaidya PD, Rodrigues AE. Insight into steam reforming of ethanol to produce hydrogen for fuel cells. Chem Eng J 2006;117:39–49.
[47] Rostrup-Nielsen JR, Christiansen LJ. Concepts in syngas manufacture. Imperial College Press; 2011.
[48] Basagiannis AC, Verykios XE. Influence of the carrier on steam reforming of acetic acid over Ru-based catalysts. Appl Catal B Environ 2008;82:77–88.
[49] Basagiannis AC, Verykios XE. Catalytic steam reforming of acetic acid for hydrogen production. Int J Hydrogen Energy 2007;32:3343–55.
[50] Güell BM, Babich I, Nichols KP, Gardeniers JGE, Lefferts L, Seshan K. Design of a stable steam reforming catalyst-A promising route to sustainable hydrogen from biomass oxygenates. Appl Catal B Environ 2009;90:38–44.
[51] Gell BM, Babich I, Lefferts L, Seshan K. Steam reforming of phenol over ni-based catalysts-A comparative study. Appl Catal B Environ 2011;106:280–6.
[52] Gorte RJ. Ceria in catalysis: from automotive applications to the water-gas shift reaction. React Kinet Catal 2010;56:1126–35.
[53] Rostrup-Nielsen JR, Sehested J, Nørskov JK. Hydrogen and synthesis gas by steam- and CO_2 reforming. Adv Catal 2002;47:65–139.
[54] Hu X, Lu G. Inhibition of methane formation in steam reforming reactions through modification of Ni catalyst and the reactants. Green Chem 2009;11:724–32.
[55] Gallezot P, Bergeret G. Handbook of heterogeneous catalysisIn Particle size and dispersion measurements. Wiley-VCH; 2010. p. 738–65 [Chap].
[56] Fogler HS. Elements of chemical reaction engineering. 4th ed. Prentice Hall; 2006.
[57] Bengaard HS, Nørskov JK, Sehested J, Clausen BS, Nielsen LP, Rostrup-Nielsen JR, et al. Steam reforming and graphite formation on Ni catalysts. J Catal 2002;209:365–84.
[58] Takanabe K, Aika K, Seshan K, Lefferts L. Sustainable hydrogen from bio-oil-Steam reforming of acetic acid as a model oxygenate. J Catal 2004;227:101–8.
[59] Zhang L, Li W, Liu J, Guo C, Wang Y, Zhang J. Ethanol steam reforming reactions over Al_2O_3-SiO_2-supported Ni–La catalysts. Fuel 2009;88:511–8.
[60] Wang P, Tanabe E, Ito K, Jia J, Morioka H, Shishido T, et al. Filamentous carbon prepared by the catalytic pyrolysis of CH_4 on Ni/SiO_2. Appl Catal A Gen 2002;231:35–44.
[61] Trimm DL. Coke formation and minimisation during steam reforming reactions. Catal Today 1997;37:233–8.
[62] Trimm DL. Catalysts for the control of coking during steam reforming. Catal Today 1999;49:3–10.
[63] Rostrup-Nielsen JR. Hydrogen via steam reforming of naphtha. Chem Eng Prog 1977;73:87–92.
[64] Rostrup-Nielsen JR. Sulfur-passivated nickel catalysts for carbon-free steam reforming of methane. J Catal 1984;85:31–43.
[65] Li J, Yu H, Yang G, Peng F, Xie D, Wang H, et al. Steam reforming of oxygenate fuels for hydrogen production: a thermodynamic study. Energy Fuels 2011;25:2643–50.
[66] Vagia EC, Lemonidou AA. Thermodynamic analysis of hydrogen production via steam reforming of selected components of aqueous bio-oil fraction. Int J Hydrogen Energy 2007;32:212–23.

[67] Vagia EC, Lemonidou AA. Hydrogen production via steam reforming of bio-oil components over calcium aluminate supported nickel and noble metal catalysts. Appl Catal A Gen 2008;351:111–21.
[68] Basagiannis AC, Verykios XE. Reforming reactions of acetic acid on nickel catalysts over a wide temperature range. Appl Catal A Gen 2006;308:182–93.
[69] Sengupta P, Khan A, Zahid MA, Ibrahim H, Idem R. Evaluation of the catalytic activity of various 5Ni/$Ce_{0.5}Zr_{0.33}M_{0.17}O_{2-\delta}$ catalysts for hydrogen production by the steam reforming of a mixture of oxygenated hydrocarbons. Energy Fuels 2012;26:816–28.
[70] Wang H, Liu Y, Wang L, Qin YN. Study of carbon deposition in steam reforming of ethanol over Co/CeO_2 catalyst. Chem Eng J 2008;145:25–31.
[71] Oliveira CF, Garcia FAC, Araujo DR, Macedo JL, Dias JL, Dias SCL. Effects of preparation and structure of cerium-zirconium mixed oxides on diesel soot catalytic combustion. Appl Catal A Gen 2012;413–414:292–300.
[72] Neyertz CA, Miro EE, Querini CA. K/CeO_2 catalysts supported on cordierite monoliths: diesel soot combustion study. Chem Eng J 2012;181–182:93–102.